
Gap function of hexagonal pnictide superconductor SrPtAs from quasiparticle interference spectrum

ALIREZA AKBARI¹ and PETER THALMEIER²

¹ *Max Planck Institute for Solid State Research, D-70569 Stuttgart, Germany*

² *Max-Planck Institute for the Chemical Physics of Solids, D-01187 Dresden, Germany*

PACS 74.20.Rp – Pairing symmetries

PACS 74.55.+v – Tunneling phenomena: single particle tunneling and STM

PACS 74.70.Xa – Pnictides and chalcogenides

Abstract – The pnictide superconductor SrPtAs has a hexagonal layered structure containing inversion symmetry. It is formed by stacking two inequivalent PtAs layers separated by Sr layers. The former have no local (in-plane) inversion symmetry and therefore a (layer-) staggered Rashba spin orbit coupling appears which splits the three Kramers degenerate bands into six quasi-2D bands. The symmetry of the superconducting state of SrPtAs is unknown. Three candidates, spin-singlet A_{1g} and E_g as well as triplet A_{2u} states have been proposed. We predict the quasiparticle interference (QPI) spectrum for these gap functions in t-matrix Born approximation. We show that distinct differences in the pattern of characteristic QPI wave vectors appear. These results may be important to determine the gap symmetry of SrPtAs by STM-QPI method.

Transition metal pnictide superconductors (SC) in particular the Fe-based systems are all of the tetragonal (orthorhombic) structure. The layered Pt-pnictide SrPtAs [1] is the first superconductor ($T_c = 2.4$ K) in that class with hexagonal structure composed of honeycomb Pt-As layers spaced by Sr layers. It may be viewed as a MgB₂ type structure with Mg sites occupied by Sr and B sites in an ordered fashion such that Pt-As alternate in the 2D honeycomb layers as well along the hexagonal c-axis. The resulting structure has an overall 3D inversion center whereas the individual layers lack 2D inversion symmetry which is not contained in the C_{3v} layer point group.

Because the electronic states at the Fermi level are mostly of Pt(5d) type with strong spin orbit coupling this leads to a peculiar electronic band structure [2]. Firstly the two inequivalent Pt-As layers have only small inter-layer hopping which results in a quasi-2D band structure consisting of three hole bands and associated Fermi surface (FS) columns. Secondly an effective 2D Rashba spin orbit coupling term leads to a large splitting of the three bands which depends on k_z in such a way that overall 3D inversion symmetry is restored.

This has consequences for the possible superconducting pair states. Due to essentially decoupled layers it is

reasonable to assume only intra-layer pairing. Then one can expect features as in the non-centrosymmetric superconductors consisting of a mixture of spin-singlet and triplet pairing of the in-plane order parameter due to lack of local 2D inversion symmetry. For the overall 3D superconducting state even or odd parity classification is restored due to the two inequivalent Sr-Pt layers. The momentum dependence of these unconventional pair states was investigated theoretically by Goryo et al [3] and it was found that even A_{1g} , E_g and odd A_{2u} states are viable candidates. However so far there is only few experimental evidence to discriminate between them [4].

One of the most powerful recent methods to determine the symmetry of the gap function is STM quasiparticle interference (QPI) technique [5]. The Fourier transform of the differential conductance scans as function of bias voltage give a fingerprint of the Fermi surface in the normal state and in addition of the \mathbf{k} -dependence of the gap function in the SC state. It has by now been successfully applied to a variety of cuprate [6–12], Fe-pnictides [13–19], and heavy fermion unconventional superconductors [20–22]. There are no STM results yet for the hexagonal pnictide SC SrPtAs.

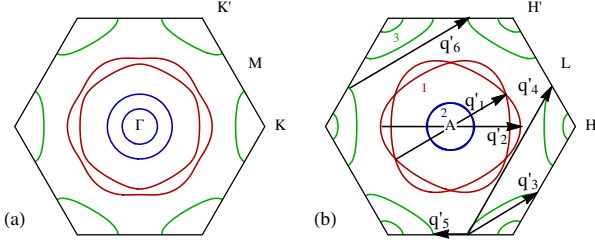


Fig. 1: (Color online) Fermi surface cuts through symmetry planes $k_z = 0$ (a) and $k_z = \pi/c$ (b). $b=1-3$ denotes three pairs of conduction bands parametrized according to Eq. (3) with parameter set $(t_1^b, t_c^b, t_{c2}^b, \mu_b, \alpha_b)$. We use [2] for $b = 1$: (1.25, 0.1, 0.05, 0.5, 0.4), for $b = 2$: (1.0, 0.1, 0.05, 2.5, 0.28) and for $b = 3$: (-0.48, 0.075, -0.03, 0.6, 0.046). \mathbf{q}_i^b are characteristic QPI scattering vectors.

Therefore in this work we propose the application of QPI to investigate the SrPtAs SC gap function. We will compare the predicted QPI spectra for the three main gap candidates discussed sofar to provide criteria for discriminating among them in future STM experiments.

The one-body Hamiltonian for three SrPtAs hole bands of mixed As(4p)-Pt(5d) character close to the Fermi energy derived in Ref. [2] and used in Refs. [3, 23] is given by

$$H_0 = \sum_{\mathbf{k}, l, l', s, b} \epsilon_{\mathbf{k}ll'}^b c_{\mathbf{k}ls}^{\dagger} c_{\mathbf{k}l's}^b + \sum_{\mathbf{k}, l, s, s', b} \alpha_b \boldsymbol{\lambda}_{\mathbf{k}l} \cdot \boldsymbol{\sigma}_{ss'} c_{\mathbf{k}ls}^{\dagger} c_{\mathbf{k}l's'}^b, \quad (1)$$

where $c_{\mathbf{k}ls}^{\dagger}$ creates conduction electrons with $b = 1, 2, 3$ denoting the (hole) band, $l, l' = 1, 2$ the inequivalent PtAs layers and $s = \pm \frac{1}{2}$ the (real) spin. Furthermore $\epsilon_{\mathbf{k}ll'}^b = \epsilon_{\mathbf{k}ll'}^b - \mu \delta_{ll'}$ ($\mu =$ chemical potential) is the Fourier transformed ($l, l' =$ layer) hopping matrix and $\alpha_b \boldsymbol{\lambda}_{\mathbf{k}l} = \alpha_b \lambda_{\mathbf{k}}^z (-1)^{(l+1)} \delta_{ll'} \hat{\mathbf{z}}$ the Rashba-type spin orbit coupling matrix for the PtAs layers which lack inversion symmetry. They are given by

$$\epsilon_{\mathbf{k}}^b = \begin{bmatrix} \epsilon_{\mathbf{k}}^b - \mu_b & \epsilon_{c\mathbf{k}} \\ \epsilon_{c\mathbf{k}}^* & \epsilon_{\mathbf{k}}^b - \mu_b \end{bmatrix}, \quad \hat{\lambda}_{\mathbf{k}}^z = \begin{bmatrix} \lambda_{\mathbf{k}}^z & 0 \\ 0 & -\lambda_{\mathbf{k}}^z \end{bmatrix}. \quad (2)$$

The intra-layer hopping is described by $\epsilon_{\mathbf{k}}^b$ and the inter-layer hybridization by $\epsilon_{c\mathbf{k}}^b$. Here $\hat{\lambda}_{\mathbf{k}}^z$ has opposite signs for $l = 1, 2$ to restore the global inversion symmetry. Its strength is given by the orbital (band) dependent Rashba coupling α_b . Explicitly [2, 3],

$$\begin{aligned} \epsilon_{\mathbf{k}}^b &= t_1^b \left[\cos k_y a + 2 \cos \frac{\sqrt{3} k_x a}{2} \cos \frac{k_y a}{2} \right] + t_{c2}^b \cos k_z c \\ |\epsilon_{c\mathbf{k}}^b|^2 &= t_c^{b2} \cos^2 \frac{k_z c}{2} \left[3 + 2 \cos k_y a + 4 \cos \frac{\sqrt{3} k_x a}{2} \cos \frac{k_y a}{2} \right] \\ \lambda_{\mathbf{k}}^z &= \sin k_y a - 2 \cos \frac{\sqrt{3} k_x a}{2} \sin \frac{k_y a}{2}. \end{aligned} \quad (3)$$

The hopping and Rashba parameters for realistic Fermi surface hole sheets [23] are given in Fig. 1. From H_0 the

normal state quasiparticle bands are

$$\Omega_{\mathbf{k}\pm}^b = (\epsilon_{\mathbf{k}}^b - \mu_b) \pm \sqrt{|\epsilon_{c\mathbf{k}}^b|^2 + \alpha_b^2 \lambda_{\mathbf{k}}^z{}^2}. \quad (4)$$

The Fermi surface cuts of the six bands ($b=1-3, \pm$) which are twofold Kramers (pseudo-spin) degenerate are shown in Fig. 1 for the normal state. The difference between $k_z = 0, \pi/c$ is due to the effect of interlayer hopping $\epsilon_{c\mathbf{k}}^b$.

Possible superconducting gap functions were proposed in Refs. [3, 23–25]. The most likely candidates are the even singlet A_{1g} and E_g and the odd triplet A_{1u} representations. Their explicit \mathbf{k} -dependence on the six bands is given by

$$\begin{aligned} A_{1g} : \Delta_{\mathbf{k}\pm}^b &= \Delta_0^b (1 + s_b e_{\mathbf{k}} \pm t'_b h_{\mathbf{k}}) \\ A_{2u} : \Delta_{\mathbf{k}\pm}^b &= \Delta_0^b (\tilde{s}_b + s_b e_{\mathbf{k}} \pm h_{\mathbf{k}}) \\ E_g : \Delta_{\mathbf{k}\pm}^b &= \sum_{s=\pm} \Delta_{0s}^b (e_{\mathbf{k}s}^s \pm t'_b h_{\mathbf{k}}^s) \end{aligned} \quad (5)$$

where $s = \pm$ denotes the time reversed chiral states of E_g with $e_{\mathbf{k}}^{\pm} = e_{\mathbf{k}1} \pm i e_{\mathbf{k}2}$ and $h_{\mathbf{k}}^{\pm} = h_{\mathbf{k}1} \pm i h_{\mathbf{k}2}$ (1, 2 correspond to real and imaginary parts). Here Δ_0^b and Δ_{0s}^b ($s = \pm$) are gap amplitudes and $(s_b, \tilde{s}_b), t'_b$ are admixture amplitudes of singlet and triplet parts. They will be assumed as band (b) independent in agreement with microscopic considerations [3]. We restrict the twofold degenerate E_g manifold to $E_g(1, 1)$ with $\Delta_{0s}^b = \Delta_0^b$. For simplicity we do not consider the chiral state $E_g(1, i)$ [25] which breaks time reversal symmetry [26]. Then $\Delta_{\mathbf{k}\pm}^b$ may be chosen real. This leads to

$$E_g(1, 1) : \Delta_{\mathbf{k}\pm}^b = 2\Delta_0^b (e_{\mathbf{k}1} \pm t'_b h_{\mathbf{k}1}). \quad (6)$$

The (real) layer gap matrices in spin space (\uparrow, \downarrow) are then given by

$$\hat{\Delta}_{\mathbf{k}1}^b = \begin{bmatrix} 0 & p \Delta_{\mathbf{k}-}^b \\ -p \Delta_{\mathbf{k}+}^b & 0 \end{bmatrix}, \quad \hat{\Delta}_{\mathbf{k}2}^b = \begin{bmatrix} 0 & \Delta_{\mathbf{k}+}^b \\ -\Delta_{\mathbf{k}-}^b & 0 \end{bmatrix}, \quad (7)$$

with p denoting the gap parity $p = 1$ for A_{1g}, E_g and $p = -1$ for A_{2u} . The form factors in Eqs. (5,6) are defined by

$$\begin{aligned} e_{\mathbf{k}} &= \cos k_y a + 2 \cos \frac{\sqrt{3} k_x a}{2} \cos \frac{k_y a}{2}, \\ h_{\mathbf{k}} &= \sin k_y a - 2 \cos \frac{\sqrt{3} k_x a}{2} \sin \frac{k_y a}{2}, \end{aligned} \quad (8)$$

for the nondegenerate (A_{1g} and A_{2u}) case and for twofold degenerate E_g gap function we have

$$\begin{aligned} e_{\mathbf{k}1} &= -\frac{1}{2} e_{\mathbf{k}}, \quad h_{\mathbf{k}1} = -\frac{1}{2} h_{\mathbf{k}}, \\ e_{\mathbf{k}2} &= \frac{\sqrt{3}}{2} \left[\cos k_y a - \cos \frac{(\sqrt{3} k_x - k_y) a}{2} \right], \\ h_{\mathbf{k}2} &= \frac{\sqrt{3}}{2} \left[\sin k_y a - \sin \frac{(\sqrt{3} k_x - k_y) a}{2} \right]. \end{aligned} \quad (9)$$

Due to even (e) and odd (h) form factors the gap elements in Eqs. (5,7) fulfill the relation $\Delta_{-\mathbf{k}\pm} = \Delta_{\mathbf{k}\mp}$. Therefore

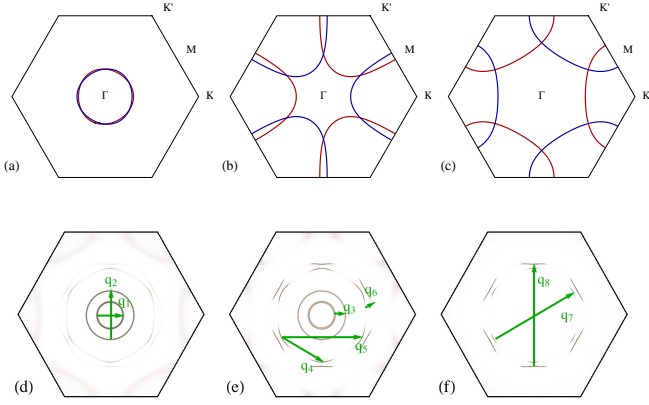


Fig. 2: (Color online) Node structure of the (a) A_{1g} , (b) A_{2u} and (c) $E_g(1,1)$ gap functions $\Delta_{\mathbf{k}\pm}^b$ in Eq. (5) (+ and - correspond to red and blue, respectively). Equal SC quasiparticle energy (Eq. (14)) surfaces for $\omega/\Delta_b^0 = 0.5$ for each of the three ($b = 1-3$) gap functions (d-f). The characteristic wave vectors \mathbf{q}_i connecting maximum curvature points are indicated. For the nondegenerate representations $\Delta_{\mathbf{k}\pm}^b$ are parametrized by Δ_b^0 and two additional parameters, namely for A_{1g} : $(s_b, t_b) = (-0.51, 0.12)$ and for A_{2u} : $(\tilde{s}_b, s_b) = (0.15, -0.18)$. For the degenerate $E_g(1,1)$ we use $t_b' = 1$. The gap amplitude was chosen as $\Delta_b^0 = 0.05$.

$$\hat{G}_A^{-1}(\mathbf{k}, i\omega_n) = \begin{bmatrix} i\omega_n - \tilde{\varepsilon}_{\mathbf{k}} - \alpha\lambda_{\mathbf{k}}^z & -p\Delta_{\mathbf{k}-} & -\varepsilon_{\mathbf{c}\mathbf{k}} & 0 \\ -p\Delta_{\mathbf{k}-}^* & i\omega_n + \tilde{\varepsilon}_{\mathbf{k}} + \alpha\lambda_{\mathbf{k}}^z & 0 & \varepsilon_{\mathbf{c}\mathbf{k}} \\ -\varepsilon_{\mathbf{c}\mathbf{k}}^* & 0 & i\omega_n - \tilde{\varepsilon}_{\mathbf{k}} + \alpha\lambda_{\mathbf{k}}^z & -\Delta_{\mathbf{k}+} \\ 0 & \varepsilon_{\mathbf{c}\mathbf{k}}^* & -\Delta_{\mathbf{k}+}^* & i\omega_n + \tilde{\varepsilon}_{\mathbf{k}} - \alpha\lambda_{\mathbf{k}}^z \end{bmatrix}, \quad (11)$$

where we define $\tilde{\varepsilon}_{\mathbf{k}}^b = \varepsilon_{\mathbf{k}}^b - \mu_b$ for each band. Then $\hat{G}_B^{-1}(\mathbf{k}, i\omega_n)$ may be obtained by substituting $\lambda_{\mathbf{k}}^z \rightarrow -\lambda_{\mathbf{k}}^z$ and $\Delta_{\mathbf{k}\pm} \rightarrow -\Delta_{\mathbf{k}\mp}$ in the above equation. Note that the model gap functions A_{1g} and A_{2u} and $E_g(1,1)$ of Eq. (6) are chosen real, i.e., $\Delta_{\mathbf{k}\pm}^* = \Delta_{\mathbf{k}\pm}$.

After inversion $\hat{G}(\mathbf{k}, i\omega_n)$ may be used to calculate the QPI spectrum $\hat{\Lambda}_0(\mathbf{q}, i\omega_n)$ which is proportional to the spatial Fourier transform of the STM differential conductance [5]. We assume that only a \mathbf{q} -independent non-magnetic impurity scattering U_c is present. For weak scattering with $U_c N_b(\mu) \ll 1$ ($N_b = \text{DOS}$ of band b) we may restrict to Born approximation. Even when this is not valid full t-matrix theory gives very similar results for the \mathbf{q} -space structure of the QPI function [27]. Within Born approximation [28, 29] it is given by $\hat{\Lambda}_0(\mathbf{q}, i\omega_n) = U_c \Lambda_0(\mathbf{q}, i\omega_n)$ with (summation over b is implied)

$$\Lambda_0(\mathbf{q}, i\omega_n) = \frac{1}{2N} \sum_{\mathbf{k}} \text{tr}_{\sigma\tau\kappa} \left[\frac{1 + \tau_3}{2} \hat{G}_{\mathbf{k}} \tau_3 \sigma_0 \kappa_0 \hat{G}_{\mathbf{k}-\mathbf{q}} \right]. \quad (12)$$

The trace is performed with respect to Nambu spin (τ), real spin (σ) and layer index (κ) where τ_3 is a Pauli matrix and σ_0, κ_0 are unit matrices.

First we discuss the purely 2D model for SrPtAs ne-

under inversion $I(\mathbf{k}, 1) = (-\mathbf{k}, 2)$, $I(\mathbf{k}, 2) = (-\mathbf{k}, 1)$ the real layer gap matrices in Eq. (7) exhibit the proper even ($p = 1$) or odd ($p = -1$) symmetry $\hat{\Delta}_{\mathbf{k}1}^b = p\hat{\Delta}_{-\mathbf{k}2}^b$ and $\hat{\Delta}_{\mathbf{k}2}^b = p\hat{\Delta}_{-\mathbf{k}1}^b$. The nodal structure of these gap functions is shown in Fig. (2a-c).

Adding the pairing term to H_0 which includes only intra-band and -layer terms this leads to a BCS model

$$H_{SC} = H_0 + \frac{1}{2} \sum_{\mathbf{k}lss'b} (\Delta_{\mathbf{k}l}^{bss'} c_{-\mathbf{k}ls}^{b\dagger} c_{\mathbf{k}ls'}^{b\dagger} + H.c.). \quad (10)$$

It is associated with the (inverse) Green's function matrix $\hat{G}^{-1} = \hat{G}_A^{-1} \otimes \hat{G}_B^{-1}$ with $\hat{G}_{A,B}^{-1} = (i\omega_n - H_{SC}^{A,B})$. Suppressing the band index (b) for the moment and expressing $H_{SC}^{A,B}$ in the spinor basis $(c_{\mathbf{k}1\uparrow}^\dagger, c_{-\mathbf{k}1\downarrow}, c_{\mathbf{k}2\uparrow}^\dagger, c_{-\mathbf{k}2\downarrow})$ for A and $(c_{\mathbf{k}1\downarrow}^\dagger, c_{-\mathbf{k}1\uparrow}, c_{\mathbf{k}2\downarrow}^\dagger, c_{-\mathbf{k}2\uparrow})$ for B we have:

glecting the dispersion along k_z setting $\varepsilon_{\mathbf{c}\mathbf{k}}^b \equiv 0$. Then the Fermi surface cut for each k_z is equivalent to that of Fig. 1b ($k_z = \pi/c$) where $\varepsilon_{\mathbf{c}\mathbf{k}}^b \equiv 0$ vanishes even for the 3D case with finite inter-layer hybridization. In the 2D model the Green's function can be obtained easily by inverting Eq. (11) due to $\varepsilon_{\mathbf{c}\mathbf{k}}^b = 0$. To perform the traces in Eq. (12) it is convenient to transform $\hat{G}(\mathbf{k}, i\omega_n)$ to reordered spinor basis $(c_{\mathbf{k}1\uparrow}^\dagger, c_{\mathbf{k}2\uparrow}^\dagger, c_{\mathbf{k}1\downarrow}, c_{\mathbf{k}2\downarrow})$ ($\tau_3 = +1$) and $(c_{-\mathbf{k}1\downarrow}, c_{-\mathbf{k}2\downarrow}, c_{-\mathbf{k}1\uparrow}, c_{-\mathbf{k}2\uparrow})$ ($\tau_3 = -1$). Then the QPI spectrum per spin and layer is obtained from Eq. (12) explicitly as

$$\Lambda_0(\mathbf{q}, i\omega_n) = \frac{1}{2N} \sum_{\mathbf{k}b\xi} \frac{(i\omega_n + \tilde{\varepsilon}_{\mathbf{k}\xi}^b)(i\omega_n + \tilde{\varepsilon}_{\mathbf{k}-\mathbf{q}\xi}^b) - \Delta_{\mathbf{k}\xi}^b \Delta_{\mathbf{k}-\mathbf{q}\xi}^{b*}}{[(i\omega_n)^2 - \tilde{E}_{\mathbf{k}\xi}^2][(i\omega_n)^2 - \tilde{E}_{\mathbf{k}-\mathbf{q}\xi}^2]}, \quad (13)$$

where the band-index b has been reintroduced. Furthermore the branches of superconducting Rashba-split quasiparticle bands are given by ($\xi = \pm$)

$$\tilde{E}_{\mathbf{k}\xi}^{b2} = \tilde{\varepsilon}_{\mathbf{k}\xi}^{b2} + |\Delta_{\mathbf{k}\xi}^b|^2; \quad \tilde{\varepsilon}_{\mathbf{k}\xi}^b = \tilde{\varepsilon}_{\mathbf{k}} - \xi \alpha_b \lambda_{\mathbf{k}}^z. \quad (14)$$

Equation (13) may be used for the calculation of the 2D QPI spectrum provided the model for $\Delta_{\mathbf{k}\pm}^b$ is specified. Here we refer to results obtained previously [27, 28] on QPI in truly non-centrosymmetric superconductors with

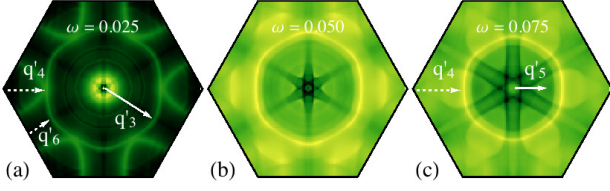


Fig. 3: (Color online) QPI spectrum (average) in the normal state for three different frequencies ω using the 2D FS model with $t_c^b = 0$. Characteristic wave vectors \mathbf{q}'_i of the normal state FS in Fig. 1b are indicated.

global inversion symmetry breaking. It was found there that generally in the expression for $\Lambda_0(\mathbf{q}, i\omega_n)$ additional Rashba coherence factors of the type $\frac{1}{2}[1 + \xi\xi'\hat{\lambda}_{\mathbf{k}}\hat{\lambda}_{\mathbf{k}'}]$ with unit vector $\hat{\lambda}_{\mathbf{k}} = \boldsymbol{\lambda}_{\mathbf{k}}/|\boldsymbol{\lambda}_{\mathbf{k}}|$ and $\xi, \xi' = \pm$ are present. However in our present case $\boldsymbol{\lambda}_{\mathbf{k}} = \lambda_z\hat{\mathbf{z}}$ has only one component and the coherence factors are just one or zero and by a suitable definition of the Rashba split bands as in Eq.(14) they do not appear explicitly in Eq.(13). For the same reason the latter also describes the QPI spectrum for magnetic scattering in Born approximation.

$$\Lambda_0(\mathbf{q}, i\omega_n) = \frac{1}{2N} \sum_{k b \xi} \frac{[(i\omega_n + \tilde{\varepsilon}_{k\xi}^b)(i\omega_n + \tilde{\varepsilon}_{k-\mathbf{q}\xi}^b) - \Delta_{k\xi}^b \Delta_{k-\mathbf{q}\xi}^b] [(i\omega_n)^2 - \tilde{E}_{k\xi}^{b2}] [(i\omega_n)^2 - \tilde{E}_{k-\mathbf{q}\xi}^{b2}]}{[(i\omega_n)^2 - \Omega_{k+}^{b2}] [(i\omega_n)^2 - \Omega_{k-}^{b2}] [(i\omega_n)^2 - \Omega_{k-\mathbf{q}+}^{b2}] [(i\omega_n)^2 - \Omega_{k-\mathbf{q}-}^{b2}]}, \quad (17)$$

where $\xi = \pm$ and $\bar{\xi} = -\xi$. The denominator in Eq. (17) is equal to the product $D_b(\mathbf{k}, i\omega_n)D_b(\mathbf{k} - \mathbf{q}, i\omega_n)$. The above expression for $\Lambda_0(\mathbf{q}, i\omega_n)$ reduces to the 2D expression in Eq. (13) for $\varepsilon_{c\mathbf{k}}^b = 0$. In contrast to Eq. (13) the momentum integral also includes the k_z - direction in Eq. (17). In the above expressions for $\Lambda_0(\mathbf{q}, i\omega_n)$ we have neglected terms $\sim |\varepsilon_{c\mathbf{k}}^b|^2, |\varepsilon_{c\mathbf{k}}^b|^4$ in the numerators since they influence only the amplitude.

Now we discuss the numerical results for the expected QPI spectrum calculated with Eq. (17). It turns out that the influence of the c-axis dispersion in the bands is of little importance due to the smallness of t_c^b in the present case of SrPtAs. Although small differences in the 3D QPI contribution of each individual k_z slice are present, the integration along k_z smoothes the differences to the simple 2D case described by Eq. (13).

We first consider the normal state whose two cuts of spectral functions (2D) are shown in Fig. (1). Particularly, in Fig. (1.b) the Fermi surface is plotted for $k_z = \pi/c$ with the typical characteristic wave vectors denoted by \mathbf{q}'_i ($i = 1-6$). The normal state DOS at the Fermi level is 74% of band-3 character [3]. The QPI should therefore be dominated by this band. Indeed this is found when considering the individual $b = 1-3$ contributions in Eq. (13).

For the numerical calculation we use the general 3D QPI by including the interlayer hopping and its resulting k_z dispersion. When $\varepsilon_{c\mathbf{k}}$ is nonzero the quasiparticle excitation spectrum is obtained by the zeroes of the determinant $D_b(\mathbf{k}, i\omega_n) = 0$ which is given by

$$D_b(\mathbf{k}, i\omega_n) = \left[(i\omega_n)^2 - \tilde{E}_{\mathbf{k}-}^{b2} \right] \left[(i\omega_n)^2 - \tilde{E}_{\mathbf{k}+}^{b2} \right] + |\varepsilon_{c\mathbf{k}}^b|^4 - 2|\varepsilon_{c\mathbf{k}}^b|^2 \left[(i\omega_n)^2 + (\tilde{\varepsilon}_{\mathbf{k}+}^b \tilde{\varepsilon}_{\mathbf{k}-}^b - p\Delta_{\mathbf{k}+}^b \Delta_{\mathbf{k}-}^b) \right]. \quad (15)$$

The 3D quasiparticle energies $\Omega_{\mathbf{k}\xi}^b$, including the effect of interlayer hopping $\varepsilon_{c\mathbf{k}}^b$ with dispersion along k_z , are obtained as

$$\Omega_{\mathbf{k}\pm}^{b2} = \frac{1}{2} (\tilde{E}_{\mathbf{k}+}^{b2} + \tilde{E}_{\mathbf{k}-}^{b2}) + |\varepsilon_{c\mathbf{k}}^b|^2 \pm \left[\frac{1}{4} (\tilde{E}_{\mathbf{k}+}^{b2} - \tilde{E}_{\mathbf{k}-}^{b2})^2 + |\varepsilon_{c\mathbf{k}}^b|^2 [(\tilde{\varepsilon}_{\mathbf{k}+}^b + \tilde{\varepsilon}_{\mathbf{k}-}^b)^2 + (\Delta_{\mathbf{k}+}^b - p\Delta_{\mathbf{k}-}^b)^2] \right]^{\frac{1}{2}}. \quad (16)$$

Here $\tilde{\varepsilon}_{\mathbf{k}+}^b + \tilde{\varepsilon}_{\mathbf{k}-}^b = 2\tilde{\varepsilon}_{\mathbf{k}}^b$. For $\Delta_{\mathbf{k}\pm}^b = 0$ we recover the quasiparticle bands $\Omega_{\mathbf{k}\xi}^b$ of the normal state in Eq.(4). Obviously for $\varepsilon_{c\mathbf{k}} = 0$ the $\Omega_{\mathbf{k}\xi}^b$ reduce to the $\tilde{E}_{\mathbf{k}\xi}^{b2}$ of Eq. (14). Then, after the inversion of Eq. (11) and performing the trace in Eq. (12) we obtain the general 3D QPI function as

The two main features in Fig. 3(a) are a large central ring and touching arcs around the zone boundary (K) points. The ring is due to \mathbf{q}'_3 and \mathbf{q}'_6 scattering (Fig. 1b) inside and between band-3 sheets (the dashed arrows are folded back into the first BZ). The arcs are due to \mathbf{q}'_4 type scattering between different band-3 sheets. When the voltage increases the ring shrinks due to the hole type bands. In addition linear features perpendicular to the hexagonal sides appear. They are due to a continuum of \mathbf{q}'_3 - \mathbf{q}'_6 scattering with the result of the averaging over the different k_z cuts.

The superconducting candidate states have very different nodal structure (Fig. 2a-c) and therefore also different quasiparticle equal energy surfaces and associated characteristic scattering wave vectors \mathbf{q}_i ($i = 1-8$) (Fig. 2.d-f). This leads to three distinct QPI spectra for the gap candidates shown in Fig. 4. They also exhibit a considerably different behavior as function of bias voltage or frequency. A few characteristic wave vectors \mathbf{q}_i associated with the equal energy surfaces in (Fig. 2.d-f) can clearly be seen in the QPI spectrum of Fig. 4 for low frequencies. In particular the faint rings with $\mathbf{q}_1, \mathbf{q}_2$ due to the small $b = 2$ band are now visible in Fig. 4(a.a) and (b.a) because the contribution of the $b=3$ band is mostly gapped out for A_{1g} and A_{2u} . For E_g in Fig. 4(c.a) however the different node structure leads to particular scattering wave vectors

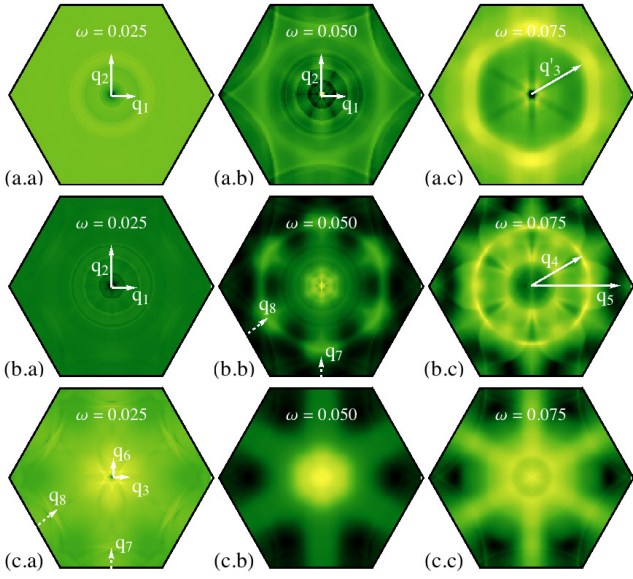


Fig. 4: (Color online) QPI spectrum (average) for the three gap candidates A_{1g} (top row (a,a-c)); A_{2u} (middle row (b,a-c)) and E_g (bottom row (c,a-c)) for three frequencies. The characteristic wave vectors \mathbf{q}_i of the equal energy SC quasiparticle surfaces in Fig. 2d-f can be identified in the structure of some QPI spectra.

(\mathbf{q}_{4-8}), on $b = 1$ sheets. In principle, $\mathbf{q}_{7,8}$ resemble the normal state $\mathbf{q}'_{1,2}$. For larger ω they also appear for A_{2u} in Fig. 4(b.b-c). At still larger $\omega = 0.075$ some features of the normal state QPI at \mathbf{q}'_3 reappear in Fig. 4(a-c.c). Also the scattering between different $b = 3$ sheets perpendicular to hexagonal BZ directions appear in the E_g QPI of Fig. 4(c.c).

To summarize we have presented the QPI theory in Born approximation for hexagonal pnictide superconductor SrPtAs. Its main hole band can be clearly identified in the normal state QPI. In the superconducting state the three candidate gap functions proposed in Ref. [3] show different types of equal energy quasiparticle sheets leading to three distinct QPI pattern and bias voltage dependences. Therefore a detailed experimental investigation of QPI in SrPtAs should be able to discriminate between the theoretically proposed gap symmetries. This is particularly desirable because recent NMR and NQR experiments [4] suggest a fully gapped spin singlet state.

REFERENCES

- [1] Y. Nishikubo, K. Kudo, and M. Nohara, 2011 *J. Phys. Soc. Jpn.*, 80 055002.
- [2] S. J. Youn, S. H. Rhim, D. F. Agterberg, M. Weinert, and A. J. Freeman, 2012 *arXiv:1202.1604*.
- [3] J. Goryo, M. H. Fischer, and M. Sigrist, 2012 *Phys. Rev. B*, 86 100507(R).
- [4] K. Matano, K. Arima, S. Maeda, Y. Nishikubo, K. Kudo, M. Nohara, and G. q. Zheng, 2014 *arXiv:1404.2154*.
- [5] L. Capriotti, D. J. Scalapino, and R. D. Sedgewick, 2003 *Phys. Rev. B*, 68 014508.
- [6] K. McElroy, R. W. Simmonds, J. E. Hoffman, D. H. Lee, J. Orenstein, H. Eisaki, S. Uchida, and J. C. Davis, 2003 *Nature (London)*, 422 592.
- [7] T. Hanaguri, Y. Kohsaka, M. Ono, M. Maltseva, P. Coleman, I. Yamada, M. Azuma, M. Takano, K. Ohishi, and H. Takagi, 2009 *Science*, 323(5916) 923–926.
- [8] J. E. Hoffman, K. McElroy, D.-H. Lee, K. M. Lang, H. Eisaki, S. Uchida, and J. C. Davis, 2002 *Science*, 297(5584) 1148–1151.
- [9] Q.-H. Wang and D.-H. Lee, 2003 *Phys. Rev. B*, 67 020511.
- [10] T. Pereg-Barnea and M. Franz, 2008 *Phys. Rev. B*, 78 020509.
- [11] M. Maltseva and P. Coleman, 2009 *Phys. Rev. B*, 80 144514.
- [12] A. V. Balatsky, I. Vekhter, and J.-X. Zhu, 2006 *Rev. Mod. Phys.*, 78 373.
- [13] T. Hanaguri, S. Niitaka, K. Kuroki, and H. Takagi, 2010 *Science*, 328(5977) 474–476.
- [14] M. P. Allan, A. W. Rost, A. P. Mackenzie, Y. Xie, J. C. Davis, K. Kihou, C. H. Lee, A. Iyo, H. Eisaki, and T. M. Chuang, 2012 *Science*, 336 563.
- [15] T.-M. Chuang, M. P. Allan, J. Lee, Y. Xie, N. Ni, S. L. Bud'ko, G. S. Boebinger, P. C. Canfield, and J. C. Davis, 2010 *Science*, 327(5962) 181–184.
- [16] Y.-Y. Zhang, C. Fang, X. Zhou, K. Seo, W.-F. Tsai, B. A. Bernevig, and J. Hu, 2009 *Phys. Rev. B*, 80 094528.
- [17] A. Akbari, J. Knolle, I. Eremin, and R. Moessner, 2010 *Phys. Rev. B*, 82 224506.
- [18] J. Knolle, I. Eremin, A. Akbari, and R. Moessner, 2010 *Phys. Rev. Lett.*, 104 257001.
- [19] H. Huang, Y. Gao, D. Zhang, and C. S. Ting, 2011 *Phys. Rev. B*, 84 134507.
- [20] A. Akbari, P. Thalmeier, and I. Eremin, 2011 *Phys. Rev. B*, 84 134505.
- [21] M. P. Allan, F. Masee, D. K. Morr, J. V. Dyke, A. W. Rost, A. P. Mackenzie, C. Petrovic, and J. C. Davis, 2013 *Nature Physics*, 9 468.
- [22] B. B. Zhou, S. Misra, E. H. da Silva Neto, P. Aynajian, R. E. Baumbach, J. D. T. E. D. Bauer, and A. Yazdani, 2013 *Nature Physics*, 9 474.
- [23] S. J. Youn, M. H. Fischer, S. H. Rhim, M. Sigrist, and D. F. Agterberg, 2012 *Phys. Rev. B*, 85 220505(R).
- [24] M. H. Fischer, F. Loder, and M. Sigrist, 2011 *Phys. Rev. B*, 84 184533.
- [25] M. H. Fischer, T. Neupert, C. Platt, A. P. Schnyder, W. Hanke, J. Goryo, R. Thomale, and M. Sigrist, 2014 *Phys. Rev. B*, 89 020509.
- [26] P. K. Biswas, H. Luetkens, T. Neupert, T. Stürzer, C. Baines, G. Pascua, A. P. Schnyder, M. H. Fischer, J. Goryo, M. R. Lees, H. Maeter, F. Brückner, H.-H. Klauss, M. Nicklas, P. J. Baker, A. D. Hillier, M. Sigrist, A. Amato, and D. Johrendt, 2013 *Phys. Rev. B*, 87 180503.
- [27] A. Akbari and P. Thalmeier, 2013 *Eur. Phys. J. B*, 86 495.
- [28] A. Akbari and P. Thalmeier, 2013 *Europhysics Letters*, 102 57008.
- [29] A. Akbari and P. Thalmeier, 2013 *Phys. Rev. B*, 88 134519.